

Adaptation controls synchrony and cluster states of coupled threshold-model neurons

Josef Ladenbauer,^{1,2,*} Judith Lehnert,^{3,†} Hadi Rankoohi,^{1,2,†}
 Thomas Dahms,³ Eckehard Schöll,³ and Klaus Obermayer^{1,2}

¹*Institut für Softwaretechnik und Theoretische Informatik,
 Technische Universität Berlin, Marchstraße 23, 10587 Berlin, Germany*

²*Bernstein Center for Computational Neuroscience Berlin, Philippstraße 13, 10115 Berlin, Germany*

³*Institut für Theoretische Physik, Technische Universität Berlin, Hardenbergstraße 36, 10623 Berlin, Germany*

We analyze zero-lag and cluster synchrony of delay-coupled non-smooth dynamical systems by extending the master stability approach, and apply this to networks of adaptive threshold-model neurons. For a homogeneous population of excitatory and inhibitory neurons we find (i) that subthreshold adaptation stabilizes or destabilizes synchrony depending on whether the recurrent synaptic excitatory or inhibitory couplings dominate, and (ii) that synchrony is always unstable for networks with balanced recurrent synaptic inputs. If couplings are not too strong, synchronization properties are similar for very different coupling topologies, i.e., random connections or spatial networks with localized connectivity. We generalize our approach for two subpopulations of neurons with non-identical local dynamics, including bursting, for which activity-based adaptation controls the stability of cluster states, independent of a specific coupling topology.

I. INTRODUCTION

Synchronization and cluster states in complex networks have been in the focus of intense research in physics, biology, neuroscience, and technology [1–7]. The key question is how the properties of the individual elements, the type of the coupling, and the topology of connections determine the collective dynamics.

A powerful technique to address this question is the master stability function (MSF) formalism [8], which has been developed for smooth coupled dynamical systems to analyze full synchrony [9–12] and cluster states with synchronized groups of elements [13–17]. In various applications, however, non-smooth dynamical systems arise [18]. Examples include electronic circuits [19, 20], hybrid control systems [21, 22], and biological networks [23–25]. Specifically in neuroscience, theoretical investigations of neuronal network activity often involve neuron models of the integrate-and-fire (IF) type, which include a discontinuity and non-smooth models of synaptic couplings between them. IF models are commonly used in computational studies of network activity [26–32], and form the hardware-elements of neuromorphic systems designed for spike-based, brain-style computations [33, 34]. In this contribution we develop an MSF formalism for delay-coupled non-smooth dynamical systems, and we demonstrate its potential by studying synchrony and cluster states for recurrent networks of adaptive IF model neurons.

II. NETWORK MODEL

Consider a network of N IF neurons which are coupled by delayed synaptic currents. We choose the adaptive exponential integrate-and-fire (aEIF) model [35], which is a two-variable neuron model that can well reproduce

a variety of subthreshold dynamics and spike patterns observed in cortical neurons [36–38]. The subthreshold dynamics of each aEIF neuron is given by ($i = 1, \dots, N$):

$$\dot{V}_i = -V_i + \exp(V_i) - w_i + I + \lambda \sum_{j=1}^N c_{ij} s_j(t - \tau), \quad (1)$$

$$\dot{w}_i = \frac{aV_i - w_i}{\tau_w}, \quad \dot{s}_i = -\frac{s_i}{\tau_s}, \quad (2)$$

where V_i is the membrane voltage, w_i is the strength of the adaptation current, and s_i is the strength of an effective synaptic (output) current. Equation (1) effectively describes the change of the membrane voltage of each neuron in reaction to the ionic currents which flow through its membrane. Five currents are taken into account (Eq. (1), left to right): The leak current, the fast sodium current at spike initiation [39], an adaptation current, which reflects slowly varying, activity-dependent potassium currents, an external driving input I , and the weighted sum of time-delayed synaptic input currents caused by the other neurons in the network with overall strength λ , weights c_{ij} , and delay τ . Equation (2), left, quantifies, how the strength of the adaptation current depends on the membrane potential, where $a \geq 0$ and τ_w is the adaptation time constant. If a neuron is activated, the adaptation current increases, counteracting this activation. Equation (2), right, describes the dynamics of the synaptic current. The activation of a model synapse decays exponentially with relaxation time τ_s .

When the membrane potential increases beyond a threshold value V_{th} , an action potential (spike) is generated. IF models do not describe the dynamics of the action potential explicitly. Instead, the synaptic output current is incremented by 1 (indicating the spike)

AUTHOR SUMMARY

How synchronous states of complex networks depend on properties of the network nodes, their coupling, and the pattern of connections is of great interest across several sciences; applications range from coupled lasers to biological networks. A powerful method to address this question is the master stability function formalism, which can be used to efficiently predict the stability of zero-lag and cluster synchrony for a wide range of connection patterns. Here we extend this formalism to coupled non-smooth dynamical systems, which, for example, occur in electronic circuits, hybrid control systems, biology, and particularly in neuroscience, where non-smooth network models have a long history.

Applying our formalism to cortical network models we identify activity-driven adaptation (a node property) as a key factor which determines the stability of synchrony largely independent of the specific pattern of connections. In particular, if couplings are not too strong, the level of adaptation that guarantees stability of synchrony in a model of a local cortical column (random connectivity) also predicts stability of global synchronous activity in a model of a cortical region (spatially structured connectivity) and vice versa. This is interesting because the adaptation properties of neurons can be changed by the neuromodulatory systems of the brain and thus provide a mechanism to control the dynamics of cortical networks.

and the membrane potential is instantaneously reset to a lower value V_r . For the aEIF neuron, the strength of the adaptation current is also changed after the spike has occurred. It is increased by a value of $b \geq 0$ implementing the mechanism of spike-based adaptation. Therefore, the aEIF model takes two mechanisms for activity-based adaptation into account, both of which are common to real cortical neurons: A subthreshold mechanism, driven by the increase of the membrane potential, and a spike-based mechanism, which is activated every time a spike has occurred. It has been shown that subthreshold adaptation can induce synchrony for pairs of symmetrically coupled excitatory neurons [40, 41] and spike-dependent adaptation can cause networks to split up into phase locked clusters [42]. Here we examine under what conditions the two adaptation mechanisms can (de)stabilize synchrony and different cluster states for a wide range of biologically plausible patterns of connections.

The network of aEIF model neurons, which we have introduced above, is a typical example of a network of non-smooth dynamical systems with time delays. These networks can be described in general by two sets of equations, one for the dynamics of the network elements between the discontinuities,

$$\dot{\mathbf{x}}_i = \mathbf{f}(\mathbf{x}_i) + \sum_{j=1}^N c_{ij} \mathbf{h}(\mathbf{x}_{j,\tau}) \quad \text{if } \varphi(\mathbf{x}_i) \neq 0, \quad (3)$$

and one for the jumps,

$$\mathbf{x}_i^+ = \mathbf{g}(\mathbf{x}_i) \quad \text{if } \varphi(\mathbf{x}_i) = 0, \quad (4)$$

$i = 1, \dots, N$, $\mathbf{x}_i \in \mathbb{R}^m$ and $\mathbf{x}_{i,\tau} \equiv \mathbf{x}_i(t - \tau)$. We assume that $\mathbf{x}_i(t)$ is piecewise continuous and that \mathbf{f} , \mathbf{g} , \mathbf{h} are differentiable vector functions [43]. φ is a scalar-valued, differentiable function that indicates the occurrence of a discontinuity, and $\mathbf{x}_i^+(t) \equiv \lim_{s \searrow t} \mathbf{x}_i(s)$ denotes a right-sided limit.

III. MASTER STABILITY FUNCTION FOR FULL SYNCHRONY

We now extend the MSF formalism to non-smooth dynamical systems as described by Eqs. (3) and (4). We assume constant row sum of the coupling matrix, $\sum_{j=1}^N c_{ij} = \bar{c} \forall i$. Then a zero-lag synchronous state exists, in which every element of the network evolves according to the same equation $\dot{\mathbf{x}} = \mathbf{f}(\mathbf{x}) + \bar{c} \mathbf{h}(\mathbf{x}_\tau) \equiv \mathbf{F}(\mathbf{x}, \mathbf{x}_\tau)$. We denote this solution by \mathbf{x}_s and the set of times at which \mathbf{x}_s changes discontinuously by $\{t_s\}$.

We next assess the stability of the fully synchronous solution \mathbf{x}_s by linearising Eqs. (3) and (4) around \mathbf{x}_s . Between the discontinuities at $t \in \{t_s\}$ and the corresponding kinks of \mathbf{x}_s at $t - \tau \in \{t_s\}$, we obtain the variational equation

$$\dot{\underline{\xi}} = [\mathbf{I}_N \otimes D\mathbf{f}(\mathbf{x}_s)] \underline{\xi} + [\mathbf{C} \otimes D\mathbf{h}(\mathbf{x}_{s,\tau})] \underline{\xi}_\tau \quad (5)$$

for the perturbations $\underline{\xi} \equiv (\xi_1, \dots, \xi_N)^T \in \mathbb{R}^{Nm}$ from the synchronous solution (cf. [12]), where $\underline{\xi}_\tau \equiv \underline{\xi}(t - \tau)$, \mathbf{I}_N is the N -dimensional unity matrix, \mathbf{C} is the coupling matrix, and \otimes denotes the Kronecker product. For non-smooth dynamical systems, however, the variational equation must be complemented by the appropriate linearized transition conditions at the times $t, t - \tau \in \{t_s\}$. Using first order approximations of the times at which $\varphi(\mathbf{x}_s + \xi_i) = 0$ and using Taylor expansions of $\mathbf{f}(\mathbf{x}_i) + \sum_{j=1}^N c_{ij} \mathbf{h}(\mathbf{x}_{j,\tau})$ around \mathbf{x}_s and \mathbf{x}_s^+ , at both t_s and $t_s + \tau$ we finally obtain (see Appendix I for a derivation):

$$\underline{\xi}^+ = [\mathbf{I}_N \otimes \mathbf{A}] \underline{\xi} \quad t \in \{t_s\}, \quad (6)$$

$$\underline{\xi}^+ = \underline{\xi} + [\mathbf{C} \otimes \mathbf{B}] \underline{\xi}_\tau \quad t - \tau \in \{t_s\}. \quad (7)$$

The matrices \mathbf{A} and \mathbf{B} are given by:

$$\mathbf{A} \equiv D\mathbf{g}(\mathbf{x}_s) + \frac{(\mathbf{F}(\mathbf{x}_s^+, \mathbf{x}_{s,\tau}) - D\mathbf{g}(\mathbf{x}_s)\mathbf{F}(\mathbf{x}_s, \mathbf{x}_{s,\tau}))D\varphi(\mathbf{x}_s)}{D\varphi(\mathbf{x}_s)\mathbf{F}(\mathbf{x}_s, \mathbf{x}_{s,\tau})} \quad (8)$$

$$\mathbf{B} \equiv \frac{(\mathbf{F}(\mathbf{x}_s, \mathbf{x}_{s,\tau}^+) - \mathbf{F}(\mathbf{x}_s, \mathbf{x}_{s,\tau}))D\varphi(\mathbf{x}_{s,\tau})}{D\varphi(\mathbf{x}_{s,\tau})\mathbf{F}(\mathbf{x}_{s,\tau}, \mathbf{x}_{s,2\tau})}. \quad (9)$$

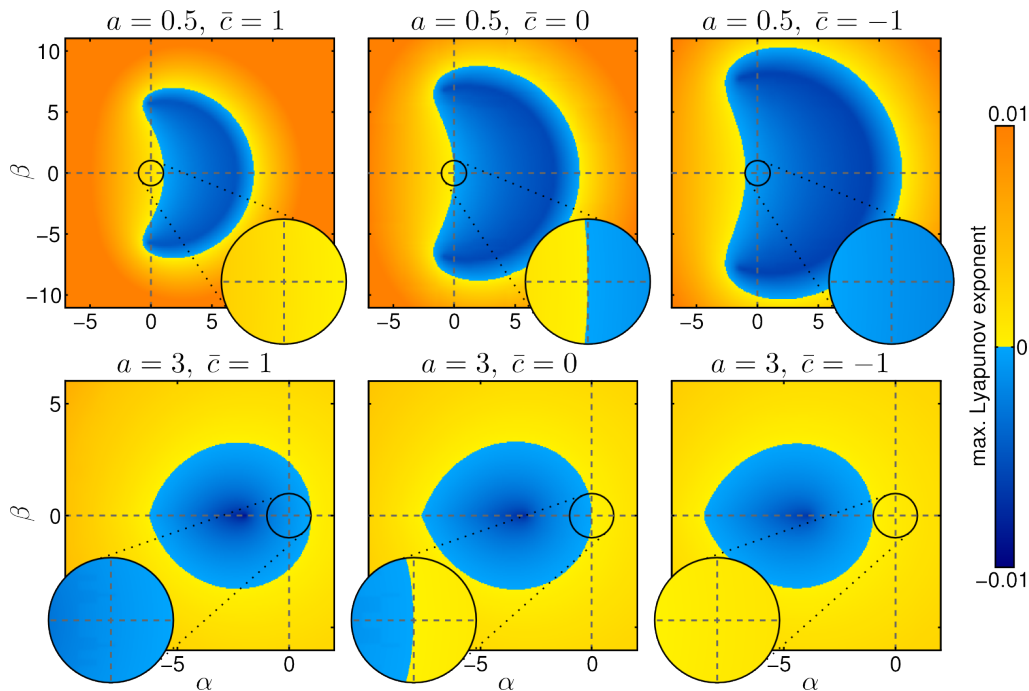


FIG. 1. (Color online) Stability of synchrony for a homogenous population of coupled aEIF neurons. The maximum Lyapunov exponent (color bar) is plotted as a function of the real (α) and imaginary (β) parts of the eigenvalues of the coupling matrix \mathbf{C} . Different panels show the results for strong (top) and weak (bottom) subthreshold adaptation, and for the excitation dominated (left), balanced (center), and inhibition dominated (right) regimes. Parameters were selected such that the dynamics of the aEIF model closely matches the regular spiking dynamics of cortical neurons [29, 37]: $\lambda = 5$, $\tau = 0.3$, $\tau_w = 10$, $\tau_s = 0.3$, $V_{th} = 5$, $V_r = -5$, $b = 2.5$. The external input I was chosen such that the oscillation period was always equal to 5. Circles indicate the unit disc in the eigenvalue plane (insets show blow-up).

Block-diagonalization of Eqs. (5)–(7) then leads to the master stability equations

$$\dot{\zeta} = Df(\mathbf{x}_s)\zeta + (\alpha + i\beta)Dh(\mathbf{x}_s, \tau)\zeta_\tau \quad t, t - \tau \notin \{t_s\}, \quad (10)$$

$$\zeta^+ = \mathbf{A}\zeta \quad t \in \{t_s\}, \quad (11)$$

$$\zeta^+ = \zeta + (\alpha + i\beta)\mathbf{B}\zeta_\tau \quad t - \tau \in \{t_s\}, \quad (12)$$

where $\zeta \equiv (\mathbf{z}^T \otimes \mathbf{I}_m)\xi$, and \mathbf{z} is the normalized eigenvector of \mathbf{C} that corresponds to the eigenvalue $\alpha + i\beta$. Hereby we separate the variational equation for perturbations in the longitudinal direction ($\alpha + i\beta = \bar{c}$) from those in the transverse directions. We can now calculate the largest Lyapunov exponent for the solution $\zeta \equiv \mathbf{0}$ as a function of α and β , which defines the MSF. Here we apply the numerical scheme proposed in [44] to obtain the Lyapunov exponents for Eqs. (10)–(12).

IV. STABILITY OF FULL SYNCHRONY FOR NETWORKS OF ADAPTIVE NEURONS

Let us first apply our MSF formalism to a homogeneous population of coupled aEIF neurons which are driven by a constant external input I . Figure 1 shows the result for six different sets of parameters. The three columns from left to right show the MSF for networks

with dominant excitatory couplings (row sum $\bar{c} = 1$), balanced excitation and inhibition ($\bar{c} = 0$), and dominant inhibitory couplings ($\bar{c} = -1$), respectively. The two rows show the MSF for neurons whose subthreshold adaptation is weak (top) and strong (bottom), respectively. If the eigenvalues of the coupling matrix lie within the unit circle (highlighted by insets in Fig. 1), stable zero-lag synchrony is predicted for excitation dominated networks of neurons with strong subthreshold adaptation and for inhibition dominated networks of neurons with weak subthreshold adaptation. An increase of spike-triggered adaptation (larger b) on the other hand does not stabilize synchrony in excitation dominated networks (not shown). For balanced networks synchrony remains unstable independently of the choice of adaptation parameters, because there are negative and positive values of the largest Lyapunov exponent in any small neighborhood of the origin [45]. In summary, we identify neuronal adaptation, which in real cortex is under top-down control of the brain's neuromodulatory systems [46–48], as one of the key factors for stabilizing or destabilizing synchrony in recurrent networks.

The MSF provides general information about the stability of the synchronous state for many different coupling matrices. We now evaluate the results shown in Fig. 1

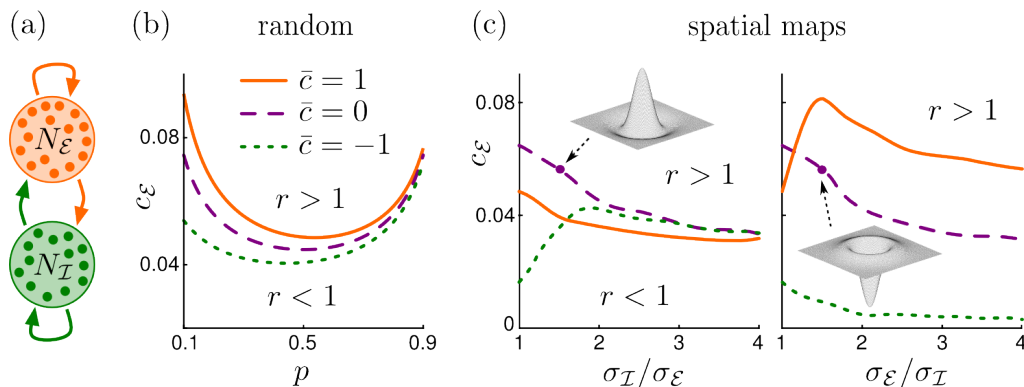


FIG. 2. (Color online) Eigenvalue spectra of coupling matrices for two biologically relevant connectivity schemes. (a) Cartoon of the network: two subpopulations of N_E excitatory (light orange) and N_I inhibitory (dark green) neurons. (b) Circle radius r computed from Eq. (13) for the random connectivity scheme. Lines of equal radius ($r = 1$) are plotted in the (p, c_E) -plane for $\bar{c} = 1, 0, -1$ (solid green, dashed violet, dotted orange lines). Parameters: $N_E = 400$, $N_I = 100$. (c) Largest absolute value r of all transverse eigenvalues, averaged over 100 sample matrices each representing a Mexican hat (left) or inverse Mexican hat (right) spatial map connectivity scheme: Excitatory and inhibitory neurons lie uniformly distributed on a two-dimensional sheet with unity edge length and periodic boundary conditions. The probability densities for excitatory and inhibitory connections are normalized Gaussian functions of the spatial distance between neurons with standard deviations σ_E and σ_I , respectively. Lines of equal absolute value ($r = 1$) are plotted with color code as in (b). Parameters: $N_E = 400$, $N_I = 100$, $p = 0.2$; $\sigma_E = 0.07$, $\sigma_I \in [0.07, 0.35]$ (left) and $\sigma_E \in [0.07, 0.35]$, $\sigma_I = 0.07$ (right). c_I in (b) and (c) via constant row sum condition.

for two qualitatively different and biologically important classes of coupling matrices. For both classes, the homogeneous population of aEIF neurons is split into two subpopulations which make excitatory ($c_E > 0$) and inhibitory ($c_I < 0$) connections only, cf. Fig. 2a. For one class of coupling matrices (random) the connections are otherwise random, i.e., connections between any two neurons in the network are chosen with equal probability. For the other class of coupling matrices (spatial maps) neurons lie on a two-dimensional sheet and the connection probability between two neurons depends on the spatial distance between them.

Figure 2b shows the results of the eigenvalue spectrum for the random connectivity scheme. One eigenvalue of the connection matrix is real and equal to the row sum \bar{c} . The other eigenvalues lie within a circle with radius

$$r = \sqrt{p(1-p)(N_E c_E^2 + N_I c_I^2)} \quad (13)$$

centered at the origin of the eigenvalue plane [49, 50]. p is the connection probability, N_E , N_I are the number of neurons in the two different subpopulations and $c_E > 0$, $c_I < 0$ are the excitatory and inhibitory coupling strengths, respectively. The curves separate the parameter regimes with $r < 1$ and $r > 1$. Figure 2c shows the corresponding results for the spatial map scheme, which were calculated numerically for both Mexican hat (range of excitatory couplings on average smaller than range of inhibitory couplings) and inverse Mexican hat (range of excitatory couplings on average larger than range of inhibitory couplings) connection matrices. The maximum size of the eigenvalues depends on the absolute values of the coupling strengths. If they are not too strong,

the eigenvalues of all three types of coupling matrices lie within the unit disc in the eigenvalue plane (highlighted in Fig. 1). We conclude that if synchrony is stable in a random network with sparse couplings, it is also stable in a spatially structured network with local couplings only. This has interesting implications for network models of cortical areas, because it implies that the stability of synchrony in a model of a local cortical column can predict the stability of global synchronous activity in a model of a spatially structured cortical map and vice versa.

V. MASTER STABILITY FUNCTION FOR CLUSTER STATES

Complete synchronization in a large network is a special phenomenon. Often cluster states emerge, for which the network splits into subgroups of elements that show isochronous synchrony internally, but there may be a phase lag or different dynamics between them [14–16]. The stability of cluster states can also be analyzed using the MSF formalism [13, 17], which we now formulate for non-smooth dynamical systems.

Consider a network which consists of two groups (\mathcal{E} , \mathcal{I}) of elements which may differ in their local dynamics (Fig. 3a). The connections of elements within and between the groups are given by the four coupling matrices $\mathbf{C}^{\mathcal{E}\mathcal{E}}$, $\mathbf{C}^{\mathcal{I}\mathcal{I}}$, $\mathbf{C}^{\mathcal{E}\mathcal{I}}$, and $\mathbf{C}^{\mathcal{I}\mathcal{E}}$, for which we assume unity

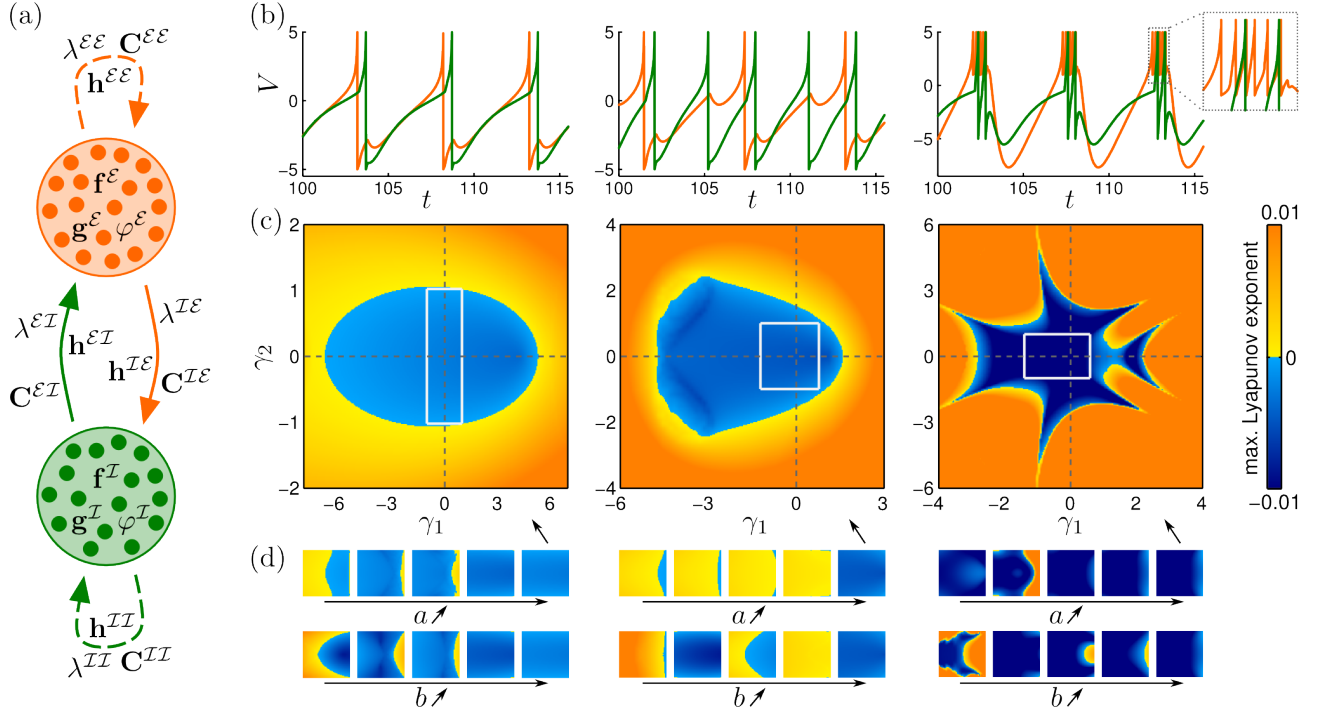


FIG. 3. (Color online) Stability of cluster states in networks with two groups of excitatory, \mathcal{E} , and inhibitory, \mathcal{I} , neurons which differ in their local dynamics. (a) Scheme of the network, according to Eqs. (14)–(15). (b) Evolution of the membrane voltage V of synchronized excitatory (light orange) and inhibitory neurons (dark green) in the network for three different parameter sets: excitatory neurons: $V_r = -5$, $I = 3.725$ (left and center), $V_r = 2$, $I = 25$ (right); inhibitory neurons: $I = 0$ (left and right), $I = 1.5$ (center). $\lambda^{\mathcal{E}\mathcal{E}} = \lambda^{\mathcal{I}\mathcal{E}} = 5$, $\lambda^{\mathcal{E}\mathcal{I}} = \lambda^{\mathcal{I}\mathcal{I}} = -5$ (left and center); $\lambda^{\mathcal{E}\mathcal{E}} = \lambda^{\mathcal{I}\mathcal{E}} = 25$, $\lambda^{\mathcal{E}\mathcal{I}} = \lambda^{\mathcal{I}\mathcal{I}} = -25$ (right). Other parameters: $a = 0.5$, $b = 2.5$, $\tau_w = 10$, $\tau_s = 0.2$, $V_{th} = 5$ for the excitatory, and $a = 0.1$, $b = 0.25$, $\tau_w = 10$, $\tau_s = 0.5$, $V_r = -5$, $V_{th} = 5$ for the inhibitory neurons; $\tau = 0.1$. (c) MSF for each of the three scenarios in (b). The maximum Lyapunov exponent is shown as a function of the real eigenvalues γ_1, γ_2 . White rectangles indicate the unit square in the eigenvalue plane. (d) MSF of the unit square as in (c), but with $a = 0.1, 0.2, 0.3, 0.4, 0.5$ (top, left to right) and $b = 0.5, 1, 1.5, 2, 2.5$ (bottom) for the excitatory neurons.

row sum. The dynamics of the network is given by:

$$\dot{\mathbf{x}}_i^k = \mathbf{f}^k(\mathbf{x}_i^k) + \lambda^{kk} \sum_{j=1}^{N_k} c_{ij}^{kk} \mathbf{h}^{kk}(\mathbf{x}_{j,\tau}^k) + \lambda^{kl} \sum_{j=1}^{N_l} c_{ij}^{kl} \mathbf{h}^{kl}(\mathbf{x}_{j,\tau}^l) \quad \text{if } \varphi^k(\mathbf{x}_i^k) \neq 0, \quad (14)$$

$$\mathbf{x}_i^{k,+} = \mathbf{g}^k(\mathbf{x}_i^k) \quad \text{if } \varphi^k(\mathbf{x}_i^k) = 0, \quad (15)$$

where $k, l \in \{\mathcal{E}, \mathcal{I}\}$ and $k \neq l$. The coupling strengths of the intra- and inter-group connections are scaled by factors $\lambda^{kk}, \lambda^{kl} \in \mathbb{R}$, respectively. In order to simplify notation, the propagation delay τ is assumed constant.

In a cluster state, all elements which belong to a group of the network are synchronized and follow the same trajectory $\mathbf{x}_s^k \equiv \mathbf{x}_i^k$, $i = 1, \dots, N_k$. Trajectories of elements which belong to different groups, however, may be different. The variational equations for the perturbations from the synchronous solution, i.e., the master stability equations, are then given by (cf. Eq. (10) for the homogenous

case):

$$\dot{\zeta}^k = D\mathbf{f}^k(\mathbf{x}_s^k)\zeta^k + \lambda^{kk}\gamma_1 D\mathbf{h}^{kk}(\mathbf{x}_{s,\tau}^k)\zeta_\tau^k + \lambda^{kl}\gamma_2 D\mathbf{h}^{kl}(\mathbf{x}_{s,\tau}^l)\zeta_\tau^l, \quad (16)$$

for $t, t-\tau \notin \{t_s^k\}$ and $t-\tau \notin \{t_s^l\}$. γ_1 and γ_2 are the eigenvalues of the block matrices $\mathbf{Q}_1 = \begin{pmatrix} \mathbf{C}^{\mathcal{E}\mathcal{E}} & \mathbf{0} \\ \mathbf{0} & \mathbf{C}^{\mathcal{I}\mathcal{I}} \end{pmatrix}$ and $\mathbf{Q}_2 = \begin{pmatrix} \mathbf{0} & \mathbf{C}^{\mathcal{E}\mathcal{I}} \\ \mathbf{C}^{\mathcal{I}\mathcal{E}} & \mathbf{0} \end{pmatrix}$, respectively [13, 17]. The variational equations - one for each group - must again be complemented by the linearized transition conditions (cf. Eqs. (11)–(12) for the homogeneous case):

$$\zeta^{k,+} = \mathbf{A}^k \zeta^k \quad t \in \{t_s^k\}, \quad (17)$$

$$\zeta^{k,+} = \zeta^k + \lambda^{kk}\gamma_1 \mathbf{B}^k \zeta_\tau^k \quad t-\tau \in \{t_s^k\}, \quad (18)$$

$$\zeta^{l,+} = \zeta^l + \lambda^{lk}\gamma_2 \mathbf{B}^k \zeta_\tau^k \quad t-\tau \in \{t_s^k\}. \quad (19)$$

\mathbf{A}^k and \mathbf{B}^k only depend on \mathbf{x}_s^k just before and after the discontinuity, see Appendix II. However, we have to require that the matrices \mathbf{Q}_1 and \mathbf{Q}_2 commute, because only then a common set of eigenvectors exists and the

pairs (γ_1, γ_2) of eigenvalues are well defined [17]. In order to assess the stability of a particular cluster state, the MSF is then evaluated for those pairs.

VI. STABILITY OF CLUSTER STATES FOR NETWORKS OF ADAPTIVE NEURONS

We apply our MSF formalism to a network of aEIF neurons, where the excitatory and the inhibitory subpopulations now have different local dynamics (cf. Fig. 3a). The aEIF neurons of the inhibitory subpopulation are weakly adaptive, and parameters are chosen such that they mimic the dynamics of the fast spiking inhibitory interneurons in the neocortex [29]. The aEIF neurons of the excitatory subpopulation are strongly adaptive, and parameters are chosen such that they either mimic the dynamics of the pyramidal neurons in the neocortex (Fig. 3b,c, left and center) or the dynamics of intrinsically bursting neurons (Fig. 3b,c, right), which - when activated - produce repeated events of rapid spiking. Bursting dynamics is mediated by spike-based adaptation for neurons with an increased reset membrane potential [37]. Figure 3c shows the MSF for real eigenvalues γ_1, γ_2 of the intra- and inter-group coupling matrices. If connections are symmetric ($c_{ij}^{kl} = c_{ji}^{lk}$, $k, l \in \{\mathcal{E}, \mathcal{I}\}$) and no autapses ($c_{ii}^{kk} = 0$) exist, the eigenvalues γ_1, γ_2 are real and lie within the unit square of the eigenvalue plane [51]. The corresponding Lyapunov exponents are all negative (Fig. 3c). However, they can become positive when subthreshold or spike-based adaptation for the excitatory neurons is decreased (Fig. 3d), indicating a potential loss of stability for the particular cluster states. We conclude that the stability of many qualitatively different cluster states is controlled by neuronal adaptation: Oscillatory activity of excitatory and inhibitory neurons with a phase lag between the two groups (Fig. 3b,c, left), inhibitory neurons spiking repetitively at a higher rate than excitatory neurons (Fig. 3b,c, center), and (3) bursting behavior (Fig. 3b,c, right). These results hold for qualitatively different classes of coupling matrices: Networks with constant all-to-all intra- and random (but symmetric, $c_{ij}^{kl} = c_{ji}^{lk}$) inter-group connections, for example, show the same synchronization behavior as one-dimensional spatial networks with local (symmetric) connectivity ($N_{\mathcal{E}} = N_{\mathcal{I}}$).

VII. CONCLUSION

In summary, we have presented an MSF formalism to study synchrony and cluster states in networks of non-smooth dynamical systems. Using our formalism we have shown that neuronal adaptation controls the stability of such network states for many qualitatively different classes of coupling matrices. Hence, our approach pro-

vides a powerful method to analyze biologically relevant dynamical states of typical cortical network models in a general setting. For example, it could be used to examine the stability of synchronous and clustered network states under influence of structural plasticity (i.e., activity-dependent changes of coupling strengths) [52, 53], irrespective of a specific coupling topology. Another interesting application of our approach in neuroscience is pulsed brain stimulation, such as transcranial magnetic stimulation [54] or deep brain stimulation [55], where our method could provide general results, e.g., when using models of coupled neuronal populations and pulse-like forcing [56, 57]. Our formalism is, however, not limited to the neuronal network level, but may be applied to a variety of diverse networks, e.g., coupled eukaryotic model cells [23], hybrid models of genetic networks [58, 59], electronic circuits such as networks of Chua's circuits [60], hybrid switching systems in production technology [61], or delay-coupled semiconductor lasers with challenging perspectives towards reservoir computing [62]. Promising applications are also anticipated for networks of interacting oscillators in the context of cognitive processing [63]. Here, the MSF can provide valuable information about the robustness of synchrony and locking dynamics against perturbations of the brain's connectivity patterns.

ACKNOWLEDGMENT

This work was supported by DFG in the framework of SFB 910.

APPENDIX I: VARIATIONAL EQUATION FOR FULL SYNCHRONY

Here we derive the transition conditions (Eqs. (6)–(9) of the paper) which complete the variational equation (5), i.e., the linearization of the network system Eqs. (3)–(4) around the synchronous solution. The derivation builds upon previous work on dynamical systems with discontinuities [64] and extends the case of uncoupled systems [41].

Let $\underline{\mathbf{x}}_s(t)$ with $\underline{\mathbf{x}}_s \equiv (\mathbf{x}_s, \dots, \mathbf{x}_s)^T : \mathbb{R} \rightarrow \mathbb{R}^{Nm}$ denote the synchronous solution of Eqs. (3)–(4), i.e., the components \mathbf{x}_s solve $\dot{\mathbf{x}} = \mathbf{f}(\mathbf{x}) + \bar{c}\mathbf{h}(\mathbf{x}_\tau)$. Furthermore, let $\underline{\boldsymbol{\xi}}$ be the solution of the linearized system Eq. (5) for small initial perturbations, $\underline{\boldsymbol{\xi}} \equiv \underline{\boldsymbol{\xi}}_0 : [t_0 - \tau, t_0] \rightarrow \mathbb{R}^{Nm}$, $\|\underline{\boldsymbol{\xi}}_0(s)\| < \epsilon$, and let t_s be the first time point $> t_0$ at which $\varphi(\mathbf{x}_s) = 0$. We define $\underline{\tilde{\mathbf{x}}} \equiv \underline{\mathbf{x}}_s + \underline{\boldsymbol{\xi}}$ and denote by t_i the time point (closest to t_s) at which $\varphi(\tilde{\mathbf{x}}_i) = 0$.

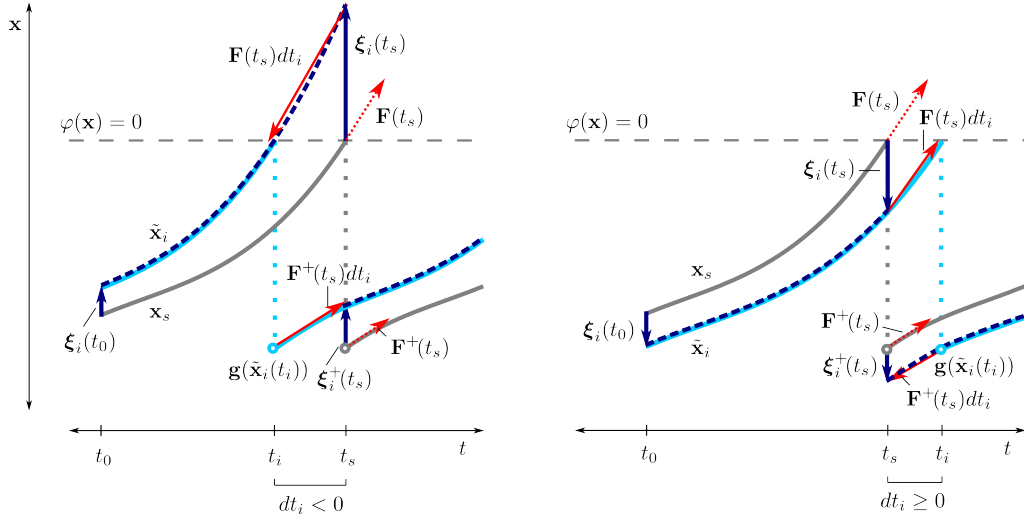


FIG. 4. (Color online) Approximation scheme for the perturbation $\xi_i^+(t_s)$ just after the discontinuity of \mathbf{x}_s , illustrated for scalar-valued functions \mathbf{x}_i ($m = 1$). Evolution of $\tilde{\mathbf{x}}_i \equiv \mathbf{x}_s + \xi_i$ (dashed dark blue lines), where \mathbf{x}_s (solid grey lines) is a component of the synchronous solution of the system Eqs. (3)–(4) and ξ_i is a solution component of Eq. (5) with initial condition $\xi \equiv \xi_0$, for $dt_i < 0$ (left) and $dt_i > 0$ (right). Note that $\tilde{\mathbf{x}}_i$ is not discontinuous at $t_i \neq t_s$, because it is not a solution component of Eqs. (3)–(4). The i -th solution component of Eqs. (3)–(4) with initial trajectory $\mathbf{x}_s + \xi_0$ is indicated (solid light blue lines). Dashed grey lines mark the set $\{\mathbf{x} | \varphi(\mathbf{x}) = 0\}$ which constitutes the threshold hyperplane here. If a solution \mathbf{x} of Eq. (3) reaches this hyperplane from below, a discontinuity occurs: $\mathbf{x}^+ = \mathbf{g}(\mathbf{x})$, cf. Eq. (4). Solid red arrows indicate the vectors $\mathbf{F}(t_s)dt_i$ and $\mathbf{F}^+(t_s)dt_i$ used in the approximation of $\xi_i^+(t_s)$. The vectors $\mathbf{F}(t_s)$ and $\mathbf{F}^+(t_s)$ are indicated by dotted red arrows.

A. Transition condition at the discontinuities

In the following we provide the linear relationship between $\xi(t_s)$ and $\xi^+(t_s)$, the perturbations just before and after the discontinuity in \mathbf{x}_s . Starting from $\tilde{\mathbf{x}}_i(t_s)$ we estimate $\tilde{\mathbf{x}}_i(t_i)$, apply the discontinuous transition Eq. (4) and then approximate $\tilde{\mathbf{x}}_i^+(t_s)$, as illustrated in Fig. 4:

$$\tilde{\mathbf{x}}_i^+(t_s) \approx \mathbf{g}(\mathbf{x}_s(t_s) + \xi_i(t_s) + \tilde{\mathbf{F}}_i(t_s)dt_i) - \tilde{\mathbf{F}}_i^+(t_i)dt_i, \quad (\text{A.1})$$

$$\approx \mathbf{x}_s^+(t_s) + D\mathbf{g}(\mathbf{x}_s(t_s))(\xi_i(t_s) + \tilde{\mathbf{F}}_i(t_s)dt_i) - \tilde{\mathbf{F}}_i^+(t_i)dt_i, \quad (\text{A.2})$$

where we have used the definitions $dt_i \equiv t_i - t_s$,

$$\tilde{\mathbf{F}}_i(t_s) \equiv \mathbf{f}(\tilde{\mathbf{x}}_i(t_s)) + \sum_{j=1}^N c_{ij} \mathbf{h}(\tilde{\mathbf{x}}_j(t_s - \tau)), \quad (\text{A.3})$$

$$\tilde{\mathbf{F}}_i^+(t_i) \equiv \mathbf{f}(\tilde{\mathbf{x}}_i^+(t_i)) + \sum_{j=1}^N c_{ij} \mathbf{h}(\tilde{\mathbf{x}}_j^+(t_i - \tau)), \quad (\text{A.4})$$

and Taylor expansion. Since dt_i , $\tilde{\mathbf{F}}_i(t_s)$ and $\tilde{\mathbf{F}}_i^+(t_i)$ are unknown we use the following approximations. First we expand $\tilde{\mathbf{F}}_i(t_s)$,

$$\tilde{\mathbf{F}}_i(t_s) \approx \mathbf{f}(\mathbf{x}_s(t_s)) + \bar{c} \mathbf{h}(\mathbf{x}_s(t_s - \tau)) \equiv \mathbf{F}(t_s). \quad (\text{A.5})$$

In order to describe dt_i we approximate $\tilde{\mathbf{x}}_i(t_i)$ as

$$\tilde{\mathbf{x}}_i(t_i) \approx \tilde{\mathbf{x}}_i(t_s) + \tilde{\mathbf{F}}_i(t_s)dt_i \quad (\text{A.6})$$

$$\approx \mathbf{x}_s(t_s) + \xi_i(t_s) + \mathbf{F}(t_s)dt_i \quad (\text{A.7})$$

and apply φ on both sides, which leads to

$$0 \approx \varphi(\mathbf{x}_s(t_s) + \xi_i(t_s) + \mathbf{F}(t_s)dt_i) \quad (\text{A.8})$$

$$\approx D\varphi(\mathbf{x}_s(t_s))(\xi_i(t_s) + \mathbf{F}(t_s)dt_i) \quad (\text{A.9})$$

We obtain a first order estimation for dt_i ,

$$dt_i \approx -\frac{D\varphi(\mathbf{x}_s(t_s))\xi_i(t_s)}{D\varphi(\mathbf{x}_s(t_s))\mathbf{F}(t_s)}. \quad (\text{A.10})$$

Next we expand $\tilde{\mathbf{F}}_i^+(t_i)$,

$$\tilde{\mathbf{F}}_i^+(t_i) = \mathbf{f}(\mathbf{g}(\tilde{\mathbf{x}}_i(t_i))) + \sum_{j=1}^N c_{ij} \mathbf{h}(\tilde{\mathbf{x}}_j^+(t_i - \tau)) \quad (\text{A.11})$$

$$\approx \mathbf{f}(\mathbf{g}(\tilde{\mathbf{x}}_i(t_s))) + \sum_{j=1}^N c_{ij} \mathbf{h}(\tilde{\mathbf{x}}_j^+(t_s - \tau)) \quad (\text{A.12})$$

$$\approx \mathbf{f}(\mathbf{x}_s^+(t_s)) + \bar{c} \mathbf{h}(\mathbf{x}_s^+(t_s - \tau)) \equiv \mathbf{F}^+(t_s). \quad (\text{A.13})$$

We substitute dt_i , $\tilde{\mathbf{F}}_i(t_s)$, $\tilde{\mathbf{F}}_i^+(t_i)$ in Eq. (A.2) and subtract $\mathbf{x}_s^+(t_s)$ on both sides to obtain the first order ap-

proximation

$$\xi_i^+ \approx \mathbf{A}\xi_i(t_s) \quad (\text{A.14})$$

$$\begin{aligned} \mathbf{A} &\equiv D\mathbf{g}(\mathbf{x}_s(t_s)) \\ &+ \frac{[\mathbf{F}^+(t_s) - D\mathbf{g}(\mathbf{x}_s(t_s))\mathbf{F}(t_s)] D\varphi(\mathbf{x}_s(t_s))}{D\varphi(\mathbf{x}_s(t_s))\mathbf{F}(t_s)} \end{aligned} \quad (\text{A.15})$$

The transition Eqs. (A.14)–(A.15) holds at all times $t_s \in \{t_s\}$ at which \mathbf{x}_s changes discontinuously.

B. Transition condition at the kinks

Next we derive the linear relationship between $\underline{\xi}(t_s + \tau)$ and $\underline{\xi}^+(t_s + \tau)$, the perturbations just before and after the kink in \mathbf{x}_s caused by the delayed coupling. We assume w.l.o.g. that the time points t_i are ordered $t_1 \leq t_2 \leq \dots \leq t_N$. Starting from $\tilde{\mathbf{x}}_i(t_s + \tau)$ we estimate first $\tilde{\mathbf{x}}_i^+(t_1 + \tau)$, then iteratively $\tilde{\mathbf{x}}_i^+(t_2 + \tau), \dots, \tilde{\mathbf{x}}_i^+(t_N + \tau)$ and finally $\tilde{\mathbf{x}}_i^+(t_s + \tau)$, see Fig. 5 for an illustration:

$$\tilde{\mathbf{x}}_i^+(t_1 + \tau) \approx \tilde{\mathbf{x}}_i(t_s + \tau) + \tilde{\mathbf{F}}_i^+(t_s + \tau)dt_1 \quad (\text{A.16})$$

$$\approx \tilde{\mathbf{x}}_i(t_s + \tau) + \mathbf{F}(t_s + \tau)dt_1, \quad (\text{A.17})$$

where we have applied Eqs. (A.3) and (A.5). Using the definition (A.4) we approximate iteratively (to first order)

$$\begin{aligned} \tilde{\mathbf{x}}_i^+(t_{k+1} + \tau) &\approx \tilde{\mathbf{x}}_i(t_k + \tau) \\ &+ \tilde{\mathbf{F}}_i^+(t_k + \tau)(dt_{k+1} - dt_k) \end{aligned} \quad (\text{A.18})$$

for $k = 1, \dots, N-1$. Since we do not know $\tilde{\mathbf{F}}_i^+(t_k + \tau)$, we approximate it as

$$\begin{aligned} \tilde{\mathbf{F}}_i^+(t_k + \tau) &\approx \mathbf{f}(\mathbf{x}_s(t_s + \tau)) + \sum_{j=1}^k c_{ij}\mathbf{h}(\mathbf{x}_s^+(t_s)) \\ &+ \sum_{j=k+1}^N c_{ij}\mathbf{h}(\mathbf{x}_s(t_s)), \end{aligned} \quad (\text{A.19})$$

where we have used that

$$\mathbf{h}(\tilde{\mathbf{x}}_j(t_k)) \approx \begin{cases} \mathbf{h}(\mathbf{x}_s^+(t_s)) & \text{for } k \geq j \\ \mathbf{h}(\mathbf{x}_s(t_s)) & \text{for } k < j, \end{cases} \quad (\text{A.20})$$

and that \mathbf{x}_s is continuous at $t_s + \tau$, assuming $t_s + \tau \notin \{t_s\}$. Using Eq. (A.18) we can now estimate $\tilde{\mathbf{x}}_i^+(t_N + \tau)$

$$\begin{aligned} \tilde{\mathbf{x}}_i^+(t_N + \tau) &\approx \tilde{\mathbf{x}}_i(t_1 + \tau) + \sum_{k=1}^{N-1} \tilde{\mathbf{F}}_i^+(t_k + \tau)(dt_{k+1} - dt_k) \\ &\approx \tilde{\mathbf{x}}_i(t_s + \tau) + \mathbf{F}^+(t_s + \tau)dt_N \\ &+ [\mathbf{h}(\mathbf{x}_s(t_s)) - \mathbf{h}(\mathbf{x}_s^+(t_s))] \sum_{j=1}^N c_{ij}dt_j, \end{aligned} \quad (\text{A.21})$$

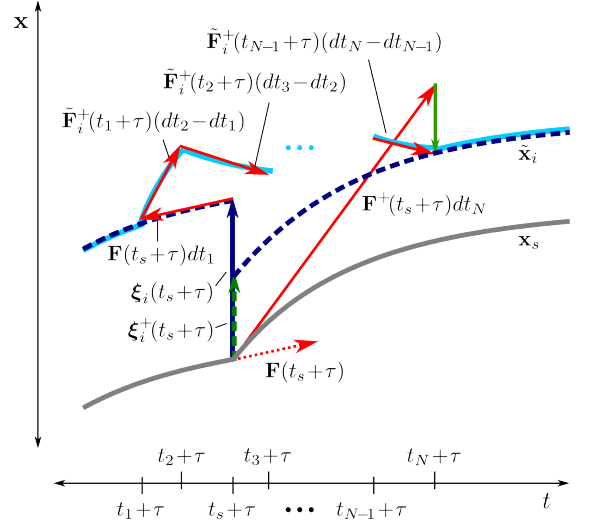


FIG. 5. (Color online) Approximation scheme for the perturbation $\xi_i^+(t_s + \tau)$ just after the kink in \mathbf{x}_s , illustrated for scalar-valued functions \mathbf{x}_i ($m = 1$). Evolution of the synchronous solution component \mathbf{x}_s (solid grey line), $\tilde{\mathbf{x}}_i \equiv \mathbf{x}_s + \xi_i$ (dashed dark blue lines) and the i -th solution component of Eqs. (3)–(4) with initial trajectory $\mathbf{x}_s + \xi_0$ (solid light blue lines). Solid red arrows indicate vectors that are used in the approximation, as explained in the text. The solid green arrow represents the difference between $\xi_i^+(t_s + \tau)$ (dashed green arrow) and $\xi_i(t_s + \tau)$ (solid dark blue arrow).

where in Eq. (A.21) we have applied Eqs. (A.17), (A.19), the definitions (A.5), (A.13) and telescopic cancelling. We use the fact that $\tilde{\mathbf{x}}_i^+(t_N + \tau)$ can also be expressed as

$$\tilde{\mathbf{x}}_i^+(t_N + \tau) \approx \tilde{\mathbf{x}}_i^+(t_s + \tau) + \mathbf{F}^+(t_s + \tau)dt_N, \quad (\text{A.22})$$

and subtract $\mathbf{F}^+(t_s + \tau)dt_N$ and $\mathbf{x}_s(t_s + \tau)$ on both sides of Eq. (A.21), which yields

$$\begin{aligned} \xi_i^+(t_s + \tau) &\approx \xi_i(t_s + \tau) + [\mathbf{h}(\mathbf{x}_s(t_s)) - \mathbf{h}(\mathbf{x}_s^+(t_s))] \\ &\cdot \sum_{j=1}^N c_{ij}dt_j. \end{aligned} \quad (\text{A.23})$$

Note that Eqs. (A.21) and (A.22) are first order approximations. Finally we substitute dt_j in Eq. (A.23) using Eq. (A.10) to obtain

$$\begin{aligned} \underline{\xi}^+(t_s + \tau) &\approx \underline{\xi}(t_s + \tau) + \left[\mathbf{I}_N \otimes \frac{\mathbf{h}(\mathbf{x}_s^+(t_s)) - \mathbf{h}(\mathbf{x}_s(t_s))}{D\varphi(\mathbf{x}_s(t_s))\mathbf{F}(t_s)} \right] \\ &\cdot [\mathbf{C} \otimes D\varphi(\mathbf{x}_s(t_s))] \underline{\xi}(t_s) \end{aligned} \quad (\text{A.24})$$

$$= \underline{\xi}(t_s + \tau) + [\mathbf{C} \otimes \mathbf{B}] \underline{\xi}(t_s), \quad (\text{A.25})$$

$$\mathbf{B} \equiv \frac{[\mathbf{h}(\mathbf{x}_s^+(t_s)) - \mathbf{h}(\mathbf{x}_s(t_s))] D\varphi(\mathbf{x}_s(t_s))}{D\varphi(\mathbf{x}_s(t_s))\mathbf{f}(\mathbf{x}_s(t_s)) + \bar{c}\mathbf{h}(\mathbf{x}_s(t_s - \tau))}. \quad (\text{A.26})$$

The transition Eq. (A.25) holds at all times $t_s + \tau$ for $t_s \in \{t_s\}$.

It should be noted that the solution $\underline{\xi}$ of the complete linearized system, Eq. (5) with transition conditions (A.14), (A.15), (A.25), approximates the evolving true perturbation given by the solution of Eqs. (3)–(4) with the small initial perturbation $\underline{\xi} \equiv \underline{\xi}_0$. The true perturbation is approximated to first order at all times except for small time intervals around t_s , $t_s + \tau$ for $t_s \in \{t_s\}$ (with duration of the same order as the magnitude of the perturbation). During these short intervals the true perturbation can be large in magnitude since generally $t_i \neq t_s$. The transition conditions guarantee that immediately after each of these intervals (which contain the instants of discontinuities and kinks) the true perturbation is approximated to first order again.

APPENDIX II: VARIATIONAL EQUATION FOR CLUSTER STATES

The transition conditions which complete the variational equation for synchronized groups of elements, i.e., the linearization of the system Eqs. (14)–(15) around the cluster state, are derived analogously to the previous section. This analogy is demonstrated by the results presented below.

The variational equation, which governs the dynamics of the perturbations $\underline{\xi} \equiv (\xi_1^{\mathcal{E}}, \dots, \xi_{N_{\mathcal{E}}}^{\mathcal{E}}, \xi_1^{\mathcal{I}}, \dots, \xi_{N_{\mathcal{I}}}^{\mathcal{I}})^T: \mathbb{R} \rightarrow$

$\mathbb{R}^{(N_{\mathcal{E}}+N_{\mathcal{I}})m}$ is given by

$$\begin{aligned} \dot{\underline{\xi}} = & \begin{pmatrix} \mathbf{I}_{N_{\mathcal{E}}} \otimes D\mathbf{f}^{\mathcal{E}}(\mathbf{x}_s^{\mathcal{E}}) & 0 \\ 0 & \mathbf{I}_{N_{\mathcal{I}}} \otimes D\mathbf{f}^{\mathcal{I}}(\mathbf{x}_s^{\mathcal{I}}) \end{pmatrix} \underline{\xi} \\ & + \begin{pmatrix} \mathbf{C}^{\mathcal{E}\mathcal{E}} \otimes D\mathbf{h}^{\mathcal{E}\mathcal{E}}(\mathbf{x}_{s,\tau}^{\mathcal{E}}) & \mathbf{C}^{\mathcal{E}\mathcal{I}} \otimes D\mathbf{h}^{\mathcal{E}\mathcal{I}}(\mathbf{x}_{s,\tau}^{\mathcal{I}}) \\ \mathbf{C}^{\mathcal{I}\mathcal{E}} \otimes D\mathbf{h}^{\mathcal{I}\mathcal{E}}(\mathbf{x}_{s,\tau}^{\mathcal{E}}) & \mathbf{C}^{\mathcal{I}\mathcal{I}} \otimes D\mathbf{h}^{\mathcal{I}\mathcal{I}}(\mathbf{x}_{s,\tau}^{\mathcal{I}}) \end{pmatrix} \underline{\xi}_{\tau} \end{aligned} \quad (\text{A.27})$$

for $t, t-\tau \notin \{t_s^{\mathcal{E}}\}$ and $t, t-\tau \notin \{t_s^{\mathcal{I}}\}$. The transition conditions for the time points, at which the synchronized elements of each group change discontinuously, are expressed as

$$\underline{\xi}^+ = \begin{pmatrix} \mathbf{I}_{N_{\mathcal{E}}} \otimes \mathbf{A}^{\mathcal{E}} & 0 \\ 0 & 0 \end{pmatrix} \underline{\xi} \quad t \in \{t_s^{\mathcal{E}}\}, \quad (\text{A.28})$$

$$\underline{\xi}^+ = \begin{pmatrix} 0 & 0 \\ 0 & \mathbf{I}_{N_{\mathcal{I}}} \otimes \mathbf{A}^{\mathcal{I}} \end{pmatrix} \underline{\xi} \quad t \in \{t_s^{\mathcal{I}}\}, \quad (\text{A.29})$$

and the transition conditions for the time points at which the delay period has passed since these (discontinuous) events, read

$$\underline{\xi}^+ = \underline{\xi} + \begin{pmatrix} \mathbf{C}^{\mathcal{E}\mathcal{E}} \otimes \mathbf{B}^{\mathcal{E}} & 0 \\ \mathbf{C}^{\mathcal{I}\mathcal{E}} \otimes \mathbf{B}^{\mathcal{E}} & 0 \end{pmatrix} \underline{\xi}_{\tau} \quad t-\tau \in \{t_s^{\mathcal{E}}\} \quad (\text{A.30})$$

$$\underline{\xi}^+ = \underline{\xi} + \begin{pmatrix} 0 & \mathbf{C}^{\mathcal{E}\mathcal{I}} \otimes \mathbf{B}^{\mathcal{I}} \\ 0 & \mathbf{C}^{\mathcal{I}\mathcal{I}} \otimes \mathbf{B}^{\mathcal{I}} \end{pmatrix} \underline{\xi}_{\tau} \quad t-\tau \in \{t_s^{\mathcal{I}}\}. \quad (\text{A.31})$$

The matrices \mathbf{A}^k and \mathbf{B}^k for $k, l \in \{\mathcal{E}, \mathcal{I}\}$, $k \neq l$, in Eqs. (A.28)–(A.31) are given by

$$\mathbf{A}^k \equiv D\mathbf{g}^k(\mathbf{x}_s^k) + \frac{[\mathbf{F}^k(\mathbf{x}_s^{k,+}, \mathbf{x}_{s,\tau}^k, \mathbf{x}_{s,\tau}^l) - D\mathbf{g}^k(\mathbf{x}_s^k)\mathbf{F}^k(\mathbf{x}_s^k, \mathbf{x}_{s,\tau}^k, \mathbf{x}_{s,\tau}^l)] D\varphi^k(\mathbf{x}_s^k)}{D\varphi^k(\mathbf{x}_s^k)\mathbf{F}^k(\mathbf{x}_s^k, \mathbf{x}_{s,\tau}^k, \mathbf{x}_{s,\tau}^l)} \quad (\text{A.32})$$

$$\mathbf{B}^k \equiv \frac{[\mathbf{F}^k(\mathbf{x}_s^k, \mathbf{x}_{s,\tau+}^k, \mathbf{x}_{s,\tau}^l) - \mathbf{F}^k(\mathbf{x}_s^k, \mathbf{x}_{s,\tau}^k, \mathbf{x}_{s,\tau}^l)] D\varphi^k(\mathbf{x}_s^k)}{D\varphi^k(\mathbf{x}_{s,\tau}^k)\mathbf{F}^k(\mathbf{x}_{s,\tau}^k, \mathbf{x}_{s,2\tau}^k, \mathbf{x}_{s,2\tau}^l)}, \quad (\text{A.33})$$

where we have used the definition

$$\mathbf{F}^k(\mathbf{x}^k, \mathbf{x}_{\tau}^k, \mathbf{x}_{\tau}^l) \equiv \mathbf{f}^k(\mathbf{x}^k) + \lambda^{kk}\mathbf{h}(\mathbf{x}_{\tau}^k) + \lambda^{kl}\mathbf{h}(\mathbf{x}_{\tau}^l). \quad (\text{A.34})$$

Note that the transition condition Eqs. (A.30)–(A.31) are caused by the delayed coupling between the elements.

* E-mail: jl@ni.tu-berlin.de

† These authors contributed equally to this work.

- [1] S. H. Strogatz, *Exploring Complex Networks*, Nature **410**, 268 (2001).
- [2] S. Boccaletti, V. Latora, Y. Moreno, M. Chavez, and D. Hwang, *Complex Networks: Structure and Dynamics*, Phys. Rep. **424**, 175 (2006).

- [3] A. Arenas, A. Díaz-Guilera, J. Kurths, Y. Moreno, and C. Zhou, *Synchronization in Complex Networks*, Phys. Rep. **469**, 93 (2008).
- [4] A. K. Engel, P. Fries, and W. Singer, *Dynamic Predictions: Oscillations and Synchrony in Top-Down Processing*, Nat. Rev. Neurosci. **2**, 704 (2001).
- [5] A. Schnitzler and J. Gross, *Normal and Pathological Oscillatory Communication in the Brain*, Nat. Rev. Neurosci. **6**, 285 (2005).
- [6] P. J. Uhlhaas and W. Singer, *Abnormal Neural Oscillations and Synchrony in Schizophrenia.*, Nat. Rev. Neurosci. **11**, 100 (2010).
- [7] X.-J. Wang, *Neurophysiological and Computational Principles of Cortical Rhythms in Cognition*, Physiol. Rev. **90**, 1195 (2010).
- [8] L. M. Pecora and T. L. Carroll, *Master Stability Functions for Synchronized Coupled Systems*, Phys. Rev. Lett. **80**, 2109 (1998).

- [9] M. Barahona and L. M. Pecora, *Synchronization in Small-World Systems*, Phys. Rev. Lett. **89**, 054101 (2002).
- [10] T. Nishikawa, A. E. Motter, Y.-C. Lai, and F. C. Hoppensteadt, *Heterogeneity in Oscillator Networks: Are Smaller Worlds Easier to Synchronize?*, Phys. Rev. Lett. **91**, 014101 (2003).
- [11] M. Chavez, D.-U. Hwang, A. Amann, H. G. E. Hentschel, and S. Boccaletti, *Synchronization is Enhanced in Weighted Complex Networks*, Phys. Rev. Lett. **94**, 218701 (2005).
- [12] M. Dhamala, V. Jirsa, and M. Ding, *Enhancement of Neural Synchrony by Time Delay*, Phys. Rev. Lett. **92**, 074104 (2004).
- [13] F. Sorrentino and E. Ott, *Network Synchronization of Groups*, Phys. Rev. E **76**, 056114 (2007).
- [14] C.-U. Choe, T. Dahms, P. Hövel, and E. Schöll, *Controlling Synchrony by Delay Coupling in Networks: From In-Phase to Splay and Cluster States*, Phys. Rev. E **81**, 025205(R) (2010).
- [15] A. A. Selivanov, J. Lehnert, T. Dahms, P. Hövel, A. L. Fradkov, and E. Schöll, *Adaptive Synchronization in Delay-Coupled Networks of Stuart-Landau Oscillators*, Phys. Rev. E **85**, 016201 (2012).
- [16] C. R. S. Williams, T. E. Murphy, R. Roy, F. Sorrentino, T. Dahms, and E. Schöll, *Experimental Observations of Group Synchrony in a System of Chaotic Optoelectronic Oscillators*, Phys. Rev. Lett. **110**, 064104 (2013).
- [17] T. Dahms, J. Lehnert, and E. Schöll, *Cluster and Group Synchronization in Delay-Coupled Networks*, Phys. Rev. E **86**, 016202 (2012).
- [18] M. Di Bernardo, C. J. Budd, A. R. Champneys, P. Kowalczyk, A. B. Nordmark, G. O. Tost, P. T. Piiroinen, D. I. Bernardo, and E. T. Al, *Bifurcations in Nonsmooth Dynamical Systems*, SIAM Rev. **50**, 629 (2008).
- [19] M. Di Bernardo, F. Garofalo, L. Glielmo, and F. Vasca, *Switchings, Bifurcations, and Chaos in DC/DC Converters*, IEEE Trans. Circuits Syst. I, Reg. Papers **45**, 133 (1998).
- [20] *Nonlinear Phenomena in Power Electronics: Bifurcations, Chaos, Control, and Applications*, edited by S. Banerjee and G. C. Verghese (Wiley-IEEE Press, New York, 2001).
- [21] H. Ye, A. N. Michel, and L. Hou, *Stability Theory for Hybrid Dynamical Systems*, IEEE Trans. Autom. Control **43**, 461 (1998).
- [22] C. G. Cassandras, D. L. Pepyne, and Y. Wardi, *Optimal Control of a Class of Hybrid Systems*, IEEE Trans. Autom. Control **46**, 398 (2001).
- [23] D. Battogtokh, K. Aihara, and J. Tyson, *Synchronization of Eukaryotic Cells by Periodic Forcing*, Phys. Rev. Lett. **96**, 011910 (2006).
- [24] K. Aihara and H. Suzuki, *Theory of Hybrid Dynamical Systems and its Applications to Biological and Medical Systems*, Phil. Trans. R. Soc. A **368**, 4893 (2010).
- [25] E. M. Izhikevich, *Dynamical Systems in Neuroscience: The Geometry of Excitability and Bursting* (MIT Press, Cambridge, MA, 2007).
- [26] E. M. Izhikevich and G. Edelman, *Large-Scale Model of Mammalian Thalamocortical Systems*, Proc. Natl. Acad. Sci. USA **105**, 3593 (2008).
- [27] T. P. Vogels and L. F. Abbott, *Gating Multiple Signals through Detailed Balance of Excitation and Inhibition in Spiking Networks*, Nat. Neurosci. **12**, 483 (2009).
- [28] A. Litwin-Kumar and B. Doiron, *Slow Dynamics and High Variability in Balanced Cortical Networks with Clustered Connections*, Nat. Neurosci. **15**, 1498 (2012).
- [29] A. Destexhe, *Self-Sustained Asynchronous Irregular States and Up-Down States in Thalamic, Cortical and Thalamocortical Networks of Nonlinear Integrate-and-Fire Neurons*, J. Comput. Neurosci. **27**, 493 (2009).
- [30] N. Brunel, *Dynamics of Sparsely Connected Networks of Excitatory and Inhibitory Spiking Neurons*, J. Comput. Neurosci. **8**, 183 (2000).
- [31] G. Gigante, M. Mattia, and P. Giudice, *Diverse Population-Bursting Modes of Adapting Spiking Neurons*, Phys. Rev. Lett. **98**, 148101 (2007).
- [32] M. Augustin, J. Ladenbauer, and K. Obermayer, *How Adaptation Shapes Spike Rate Oscillations in Recurrent Neuronal Networks*, Front. Comput. Neurosci. **7**, 1 (2013).
- [33] G. Indiveri, E. Chicca, and R. Douglas, *A VLSI Array of Low-Power Spiking Neurons and Bistable Synapses with Spike-Timing Dependent Plasticity*, IEEE Trans. Neural Netw. **17**, 211 (2006).
- [34] S. H. Jo, T. Chang, I. Ebong, B. B. Bhadviya, P. Mazumder, and W. Lu, *Nanoscale Memristor Device as Synapse in Neuromorphic Systems*, Nano Lett. **10**, 1297 (2010).
- [35] R. Brette and W. Gerstner, *Adaptive Exponential Integrate-and-Fire Model as an Effective Description of Neuronal Activity*, J. Neurophysiol. **94**, 3637 (2005).
- [36] The aEIF neuron model employed here uses dimensionless variables. It is a rescaled variant of the original model, but with fewer parameters, see J. Touboul and R. Brette, *Dynamics and Bifurcations of the Adaptive Exponential Integrate-and-Fire Model*, Biol. Cybern. **99**, 319 (2008).
- [37] R. Naud, N. Marcille, C. Clopath, and W. Gerstner, *Firing Patterns in the Adaptive Exponential Integrate-and-Fire Model*, Biol. Cybern. **99**, 335 (2008).
- [38] R. Jolivet, F. Schürmann, T. K. Berger, R. Naud, W. Gerstner, and A. Roth, *The Quantitative Single-Neuron Modeling Competition*, Biol. Cybern. **99**, 417 (2008).
- [39] The fast sodium current of the aEIF model includes the effect of the sodium current, which is responsible for the generation of spikes.
- [40] G. B. Ermentrout, M. Pascal, and B. S. Gutkin, *The Effects of Spike Frequency Adaptation and Negative Feedback on the Synchronization of Neural Oscillators*, Neural Comput. **13**, 1285–1310 (2001).
- [41] J. Ladenbauer, M. Augustin, L. Shiau, and K. Obermayer, *Impact of Adaptation Currents on Synchronization of Coupled Exponential Integrate-and-Fire Neurons*, PLoS Comput. Biol. **8**, e1002478 (2012).
- [42] Z. P. Kilpatrick and G. B. Ermentrout, *Sparse Gamma Rhythms Arising through Clustering in Adapting Neuronal Networks*, PLoS Comput. Biol. **7**, e1002281 (2011).
- [43] Note that \mathbf{h} does not depend on \mathbf{x}_i in Eq. (3). The following derivation, however, can be extended to coupling functions $\mathbf{h}(\mathbf{x}_i, \mathbf{x}_j, \tau)$ in a straightforward way.
- [44] J. D. Farmer, *Chaotic Attractors of an Infinite-Dimensional Dynamical System*, Physica D **4**, 366 (1982).
- [45] We observed this behavior for a wide range of model parameters.
- [46] D. A. McCormick, *Neurotransmitter Actions in the Thalamus and Cerebral Cortex and their Role in Thalamocortical Activity*, Prog. Neurobiol. **39**, 337 (1992).

- [47] L. F. Abbott and S. B. Nelson, *Synaptic Plasticity: Taming the Beast*, Nat. Neurosci. **3**, 1178 (2000).
- [48] A. Destexhe and E. Marder, *Plasticity in Single Neuron and Circuit Computations*, Nature **431**, 789 (2004).
- [49] R. T. Gray and P. A. Robinson, *Stability and Structural Constraints of Random Brain Networks with Excitatory and Inhibitory Neural Populations*, J. Comput. Neurosci. **27**, 81 (2009).
- [50] K. Rajan and L. Abbott, *Eigenvalue Spectra of Random Matrices for Neural Networks*, Phys. Rev. Lett. **97**, 188104 (2006).
- [51] This follows from Gershgorin's circle theorem, because the coupling matrices \mathbf{C}^{kl} ($k, l \in \{\mathcal{E}, \mathcal{I}\}$) all have non-negative entries with unity row sum. Excitatory and inhibitory interactions are generated via the overall coupling parameters $\lambda^{k\mathcal{E}} > 0$ and $\lambda^{k\mathcal{I}} < 0$.
- [52] H. Câteau, K. Kitano, and T. Fukai, *Interplay between a Phase Response Curve and Spike-Timing-Dependent Plasticity Leading to Wireless Clustering*, Phys. Rev. E **77**, 051909 (2008).
- [53] E. V. Lubenov and A. G. Siapas, *Decoupling through Synchrony in Neuronal Circuits with Propagation Delays*, Neuron **58**, 118 (2008).
- [54] M. Hallett, *Transcranial Magnetic Stimulation and the Human Brain*, Nature **406**, 147 (2000).
- [55] M. L. Kringelbach, N. Jenkinson, S. Owen, and T. Aziz, *Translational Principles of Deep Brain Stimulation*, Nat. Rev. Neurosci. **8**, 623 (2007).
- [56] S. K. Esser, S. L. Hill, and G. Tononi, *Modeling the Effects of Transcranial Magnetic Stimulation on Cortical Circuits*, J. Neurophysiol. **94**, 622 (2005).
- [57] P. Tass, *A Model of Desynchronizing Deep Brain Stimulation with a Demand-Controlled Coordinated Reset of Neural Subpopulations*, Biol. Cybern. **89**, 81 (2003).
- [58] T. J. Perkins, R. Wilds, and L. Glass, *Robust Dynamics in Minimal Hybrid Models of Genetic Networks*, Phil. Trans. R. Soc. A **368**, 4961 (2010).
- [59] W. Zhang, Y. Tang, J. Fang, and W. Zhu, *Exponential Cluster Synchronization of Impulsive Delayed Genetic Oscillators with External Disturbances*, Chaos **21**, 043137 (2011).
- [60] P. De Lellis, M. Di Bernardo, and F. Garofalo, *Synchronization of Complex Networks through Local Adaptive Coupling*, Chaos **18**, 037110 (2008).
- [61] A. Amann, K. Peters, U. Parlitz, A. Wacker, and E. Schöll, *Hybrid Model for Chaotic Front Dynamics: From Semiconductors to Water Tanks*, Phys. Rev. Lett. **91**, 066601 (2003).
- [62] M. C. Soriano, J. Garca-Ojalvo, C. R. Mirasso, and I. Fischer, *Complex Photonics: Dynamics and Applications of Delay-Coupled Semiconductors Lasers*, Rev. Mod. Phys. **85**, 421 (2013).
- [63] G. Deco, V. Jirsa, and A. R. McIntosh, *Emerging Concepts for the Dynamical Organization of Resting-State Activity in the Brain*, Nat. Rev. Neurosci. **12**, 43 (2011).
- [64] P. C. Mueller, *Calculation of Lyapunov Exponents for Dynamic Systems with Discontinuities*, Chaos Soliton. Fract. **5**, 1671 (1995).